

EXPERIMENTAL STUDY

Could *Peganum harmala* be effective in the treatment of COVID-19?

Tuzun B¹, Nasibova T², Garaev E², Sayin K¹, Ataseven H³

Chemistry Department, Science Faculty, Sivas Cumhuriyet University, Sivas, Turkey.
theburaktuzun@yahoo.com

ABSTRACT

BACKGROUND: Predominant molecules in *Peganum harmala* leaves were detected using gas chromatography-mass spectrometry (GC-MS). Based on the results of this analysis, most alkaloids, flavonoids and triterpenoids in found *P. harmala* was compiled from the literature in order to develop and lead the production of effective inhibitor drugs for ACE2, main protease, and RNA dependent RNA polymerase (RdRp) proteins of SARS-CoV-2 virus, which is today's most contagious and deadly disease.

AIM: By comparing FDA-approved drugs used in the treatment of COVID-19, we aimed to determine whether the molecules in *P. harmala* are effective against SARS CoV-2 *in silico*.

RESULTS AND CONCLUSION: *P. harmala* molecules were selected as drug candidates from the PubChem web tool. Afterwards, molecular docking calculations of these inhibitor molecules were made with Maestro Molecular modeling program by Schrödinger. The comparison of molecules with high inhibitory activities with FDA-approved drugs was made. With molecular mechanics Poisson-Boltzmann surface area (MM-PBSA) calculations, docking calculations of molecules that have high inhibitory activity, were tried to be verified by calculations in the range of 0-100 nanoseconds (Tab. 4, Fig. 6, Ref. 53). Text in PDF www.elis.sk.

KEY WORDS: SARS CoV-2, *Peganum harmala*, Gas Chromatography-Mass spectrometry, molecular docking.

Introduction

P. harmala (*Nitrariaceae*) is a perennial herb found in the Middle East and Central Asia, Europe, and North America (1). It is widely used in folk medicine for the common cold, fever, asthma, bronchitis, diarrhea, etc. These properties are associated with anti-inflammatory, bronchodilating, analgesic, and antiviral effects (2). The positive effects of *P. harmala* against influenza A virus, Newcastle disease virus (NDV) (3), dengue virus (4), herpes simplex virus type 1 (HSV-1, oral herpes), herpes simplex virus type 2 (HSV-2, genital herpes) (5), human cytomegalovirus (HCMV, human herpesvirus 5 (HHV-5), coxsackie B virus type 3 (6), human immunodeficiency virus (HIV) (7) have been proven in *in vitro* experiments.

Most diseases caused by these viruses have indications similar to COVID-19. Influenza A virus is particularly similar to corona-

virus due to symptoms, and the co-infection of these two viruses among the population is worsening the health status (8). Coronavirus-like symptoms also appear in dengue disease, which is caused by the dengue virus (9). HSV is a common pathogen capable of causing an infection of the respiratory tract, HSV pneumonia or tracheobronchitis is the most common type (10). HCMV infection of the respiratory tract results in pneumonitis (11). In 80 % of cases, all patients had irregular lung images marked by ground-glass opacity/consolidation like COVID-19 (12). Coxsackie B virus symptoms include headache, fever, sore throat, stomach discomfort, intense weakness, and chest pain, which is close to coronavirus disease symptoms (13). In 20 % of HIV-infected patients, respiratory viruses occur which are observed with breath shortness and coughing (14). At the same time, influenza A (15), dengue (16), HIV (17), coxsackie B (18), and Newcastle viruses (19) have an RNA structure such as coronavirus, and β -carboline alkaloids that predominate in *P. harmala* can bind to both RNA and DNA (20) (Figs 1, 2).

Materials and methods*Sample collection*

P. harmala L. leaves were collected in Baku, Azerbaijan in August 2019 from the natural habitat of the plant.

Chemicals and reagents

Ethanol and methanol were purchased from Merck (Germany), 0.45 μ m sterile syringe filters supplied by Isolab (Germany).

¹Chemistry Department, Science Faculty, Sivas Cumhuriyet University, Sivas, Turkey, ²General and Toxicological Chemistry Department, Azerbaijan Medical University, Baku, Azerbaijan, and ³Department of Gastroenterology, Faculty of Medicine, Sivas Cumhuriyet University, Sivas, Turkey
Address for correspondence: B. Tuzun, Chemistry Department, Science Faculty, Sivas Cumhuriyet University, 58140 Sivas, Turkey.

Acknowledgments: This work is supported by the Scientific Research Project Fund of Sivas Cumhuriyet University under project number RGD-020. This research was made possible by TUBITAK ULAKBIM, High Performance and Grid Computing Center (TR-Grid e-Infrastructure)



Fig. 1. *P. harmala* capsules.

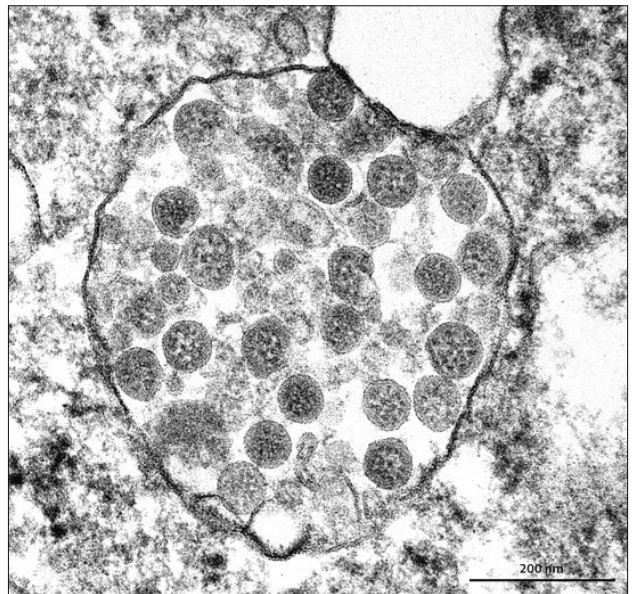


Fig. 2. Coronaviruses (perceiving as black dots) clustered in a cell membrane (21).

Extract preparation

Disease-free leaves were shade-dried at room temperature for 14 days and ground into fine powder by using a mechanical grinder. 100 g of the powder was extracted three times with 95 % ethanol with the 1:10 m/v ratio of plant material to solvent for 3 days. The ethanolic extract was evaporated to obtain concentrated dry residue (20.82 g). This mass was treated with distilled water and the resulting aqueous extract was evaporated in a large open-mouthed bowl at 40 °C until a dry residue (5.1 g) was obtained. To prepare the analysis solution 0.2 g of this mass was taken and 2 ml of methanol was added. At this stage, the dry residue was easily soluble in methanol. The resulting solution was filtered using a 0.45 µm sterile syringe filter and was transferred to the vial for identification of various phytochemical compounds.

Gas chromatography-mass spectrometry (GC-MS) analysis

GC-MS analysis was performed on a quadrupole Shimadzu GCMS-QP2010 Ultra gas chromatograph-mass spectrometer equipped with Rxi-5Sil MS Column (30 m L, 0.25 mm I.D., df = 0.25 µm) (Restek Corporation, P/N: 13623) under the following conditions: oven temperature program is regulated as follows: 60 °C (1 min) – 160 °C at 25 °C/min, 160 °C – 240 °C at 4 °C/min, 240 °C – 290 °C at 10 °C/min, finally isothermal regime at 290 °C for 11 min. The carrier gas was helium with a constant flow of 1 ml/min. The volume of the injected sample was 2 µL through an AOC-5000 Plus, AOC-20i/s auto-sampler using the splitless injection technique, the ionization energy of 70 eV was employed in the electronic ionization mode. The identification of the compounds was realized by matching their fragmentation patterns with Wiley Registry 9th and NIST11 GC-MS libraries.

Molecular docking

All inhibitor molecules containing *P. harmala* were optimized with the Gaussian software program (22). Files with extension *.sdf were obtained from these optimized structures. Later, these files were calculated by the Maestro Molecular modeling platform (version 12.2) by Schrödinger (23). The program studied consists of many modules. These modules are used to prepare proteins with inhibitor molecules for their interactions with inhibitor molecules. In the first module, the protein prep module (24) is used to prepare proteins. The LigPrep module (25) was used to find many conformers of inhibitor molecules and to prepare inhibitor molecules for calculations. Next, the Glide ligand docking module (26) was used to interact with the prepared inhibitor molecules and the proteins with each other. This module is very important to examine the interaction of proteins with inhibitor molecules in detail. After examining these interactions, ADME/T analysis (absorption, distribution, metabolism, excretion, and toxicity) was performed to predict the effects and responses of inhibitor molecules on human metabolism. The Qik-prop module (27) of the Schrödinger software module was used for this analysis.

MM-PBSA calculations

After the molecular docking calculations, Molecular mechanics Poisson-Boltzmann surface area (MM-PBSA) calculations were made to examine the interactions between molecules and proteins in nanoseconds. These calculations can calculate many parameters such as binding free energy between molecules and proteins, van der Waals energy, electrostatic energy, kinetic energy, and potential energy loads. These calculations were made using Nanoscale Molecular Dynamics (NAMD) (28) and Visual Molecular Dynamics (VMD) (29) software programs. As a result

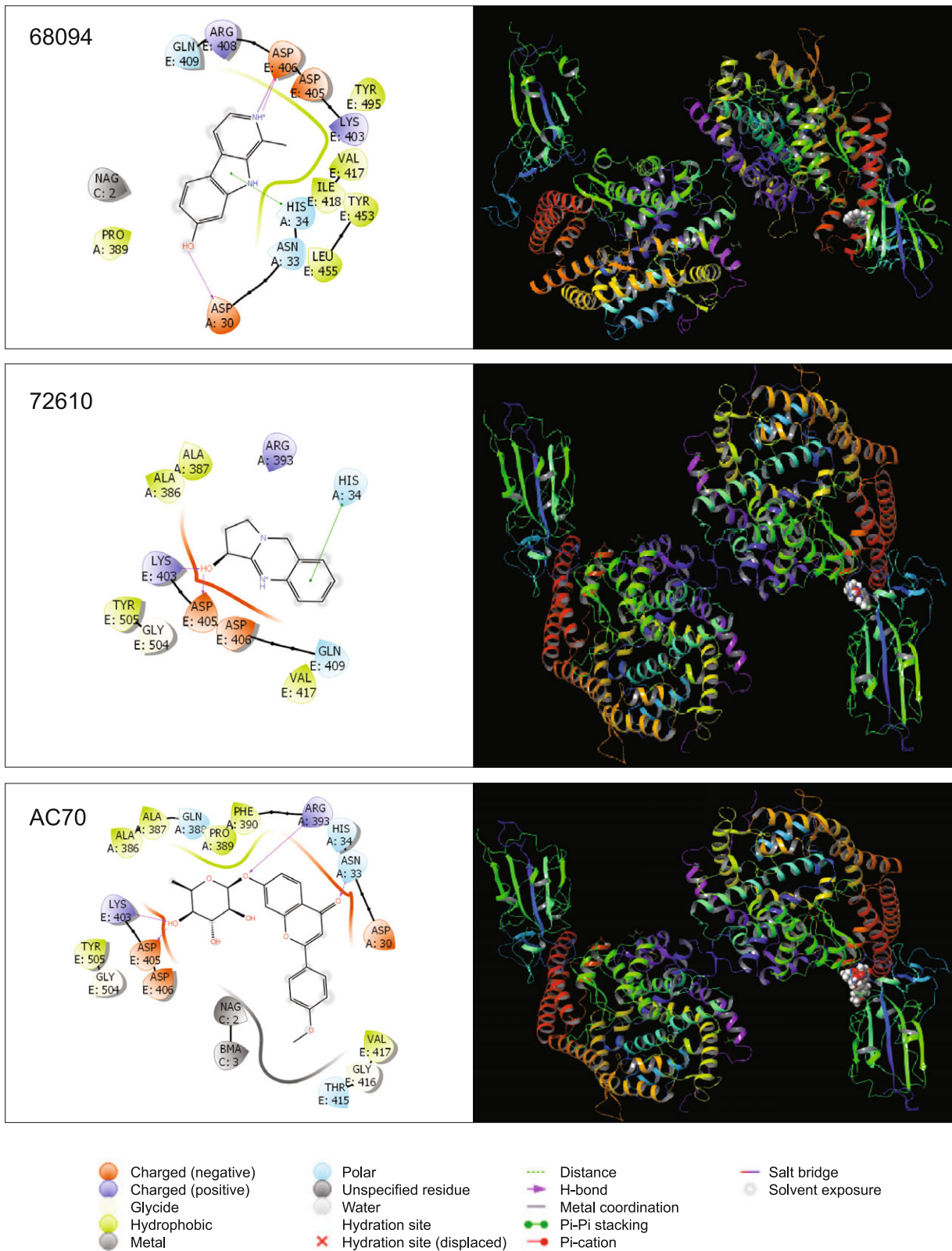


Fig. 3. Illustration of the interaction of molecules with the 6VW1 protein of the SARS-CoV-2 virus.

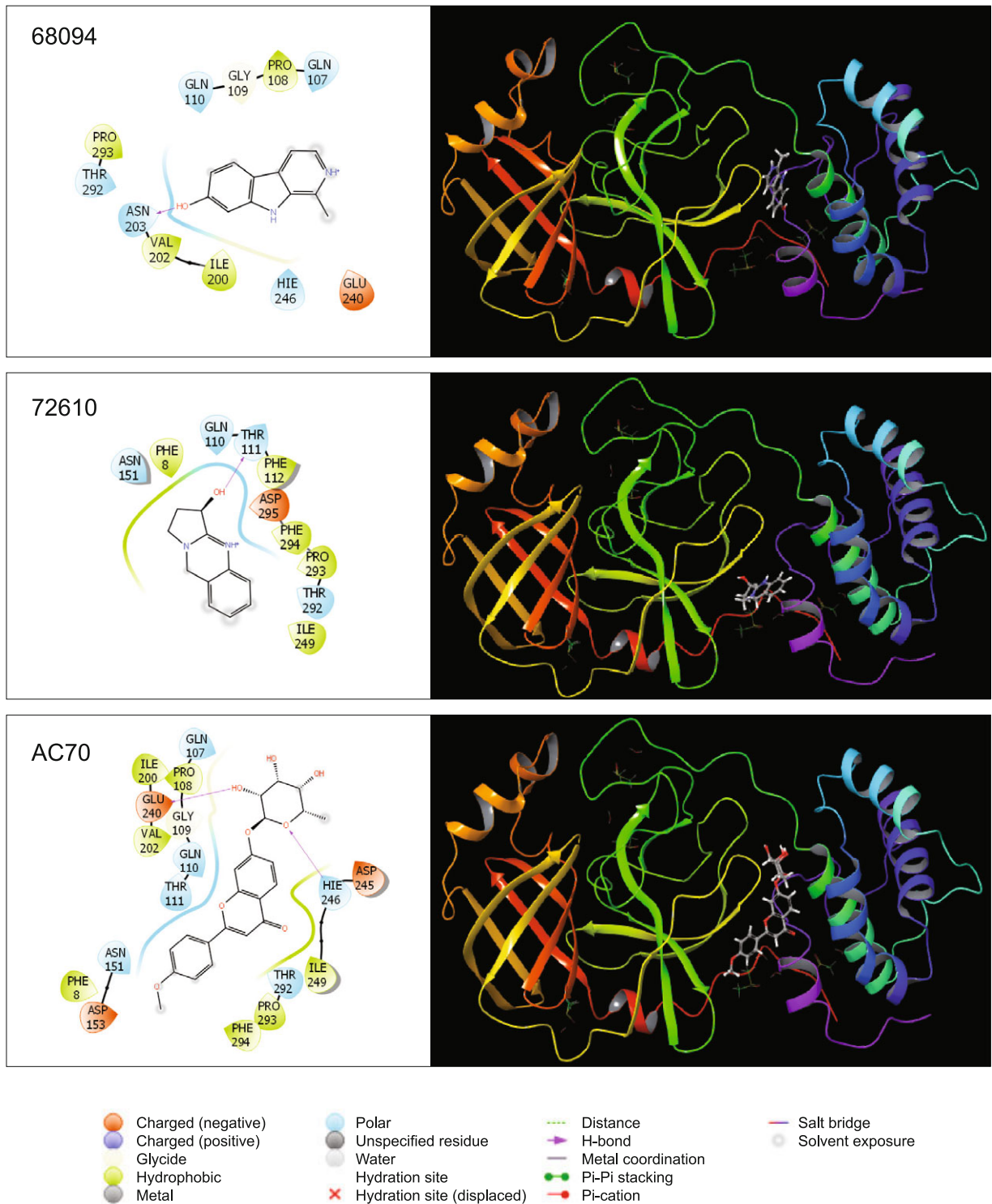


Fig. 4. Illustration of the interaction of molecules with the 7BU protein of the SARS-CoV-2 virus.

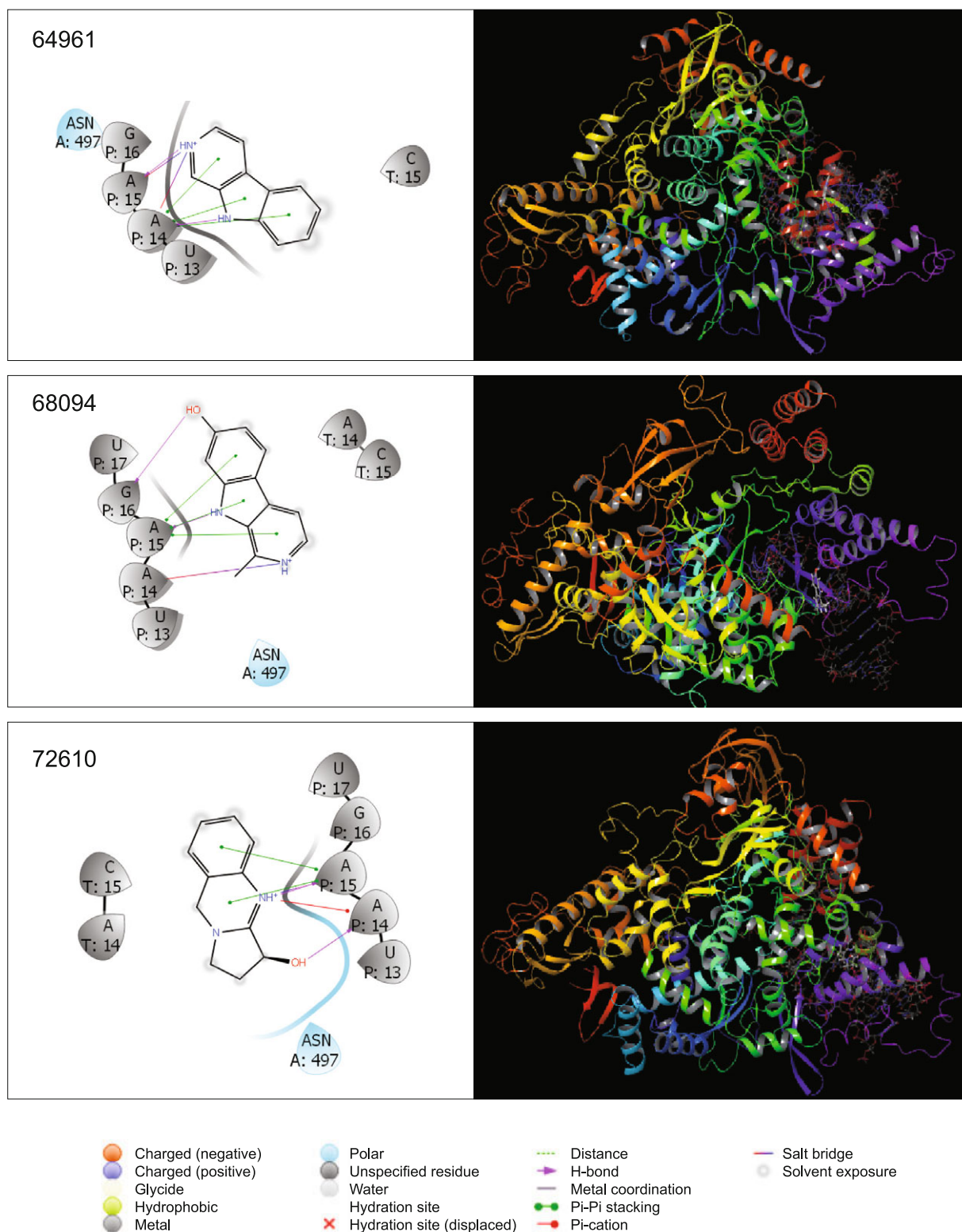


Fig. 5. Illustration of the interaction of molecules with the 7BV2 protein of the SARS-CoV-2 virus.

Tab. 1. All parameters calculated for interaction between inhibitor molecules and proteins.

	Docking score	Glide ligand efficiency	Glide ecoul	Glide emodel	Glide energy	Glide einternal	Glide posenum
6VW1							
AC7O	-6.01	-0.20	-0.31	-28.07	-18.98	-56.57	-47.05
72610	-5.73	-0.41	-0.34	-15.70	-8.87	-37.58	-24.56
68094	-5.55	-0.37	-0.36	-15.04	-11.35	-38.34	-26.39
3565	-5.43	-0.36	-0.50	-14.69	-11.01	-34.70	-25.70
64961	-5.16	-0.40	-0.23	-12.89	-7.11	-29.28	-20.00
7BUY							
72610	-6.89	-0.49	-0.40	-18.02	-12.63	-48.28	-30.65
AC7O	-6.61	-0.22	-0.26	-35.23	-8.93	-59.05	-44.15
68094	-5.96	-0.40	-0.32	-20.86	-8.89	-44.64	-29.75
91522	-5.62	-0.40	-0.32	-16.68	-8.57	-38.81	-25.24
107838	-5.48	-0.42	-0.13	-14.73	-7.52	-35.83	-22.25
7BV2							
68094	-7.28	-0.49	-0.29	-17.17	-24.82	-72.61	-41.99
72610	-6.86	-0.49	-0.41	-17.02	-21.04	-67.14	-38.06
64961	-6.66	-0.51	-0.34	-16.87	-19.31	-64.26	-36.18
AC7O	-6.46	-0.22	-0.29	-25.95	-22.21	-67.35	-48.16
107838	-6.25	-0.48	-0.35	-18.32	-17.31	-61.41	-35.63
91522	-6.08	-0.43	-0.22	-19.74	-16.19	-59.68	-35.93
68261	-5.80	-0.41	-0.43	-22.85	-5.08	-37.82	-27.92
3565	-5.47	-0.36	-0.29	-23.89	-7.65	-40.85	-31.54

of the calculations, each calculated energy parameter includes many quantum chemical energy units, which are van der Waals energy, electrostatic energy, polar contribution to internal energy, and solvent energy.

Result and discussion

GC-MS analysis

The current research was designed to classify active compounds present in *P. harmala* leaves using the GC-MS method. As a result, different chemical groups were identified. These groups include alkaloids and quinoline, quinazoline, indole, β -carboline derivatives, fatty acids, and their derivatives, carboxylic acid derivatives, alcohols, common basic phytochemicals with other plants. Vasicine, vasicinone, harmine, harmol were the most abundant alkaloids in this plant material. 4-(3-propynyloxy)quinazoline alkaloid is rarely found in *P. harmala* and has also been determined in our research. These alkaloids have been observed in higher amounts in *P. harmala* extract than in other groups of substances. Besides, some quinoline, quinazoline, indole, and β -carboline derivatives were also identified which were observed in the *P. harmala* for the first time and these are structurally similar to the known alkaloids in this plant. Based on the high content of alkaloids in *P. harmala*, a list of especially alkaloids found in this species, as well as flavonoids and triterpenoids, was collected from the literature, and molecular docking analysis of these molecules was performed against the SARS-CoV-2 proteins.

Docking studies

Today, it is seen in recent studies that experimental procedures have been started using the findings obtained as a result of theoretical calculations (30–32). In these studies, theoretical prelimi-

nary calculations were made and molecules with high chemical and biological activity were identified and these molecules were synthesized. In fact, the researchers tried to develop these molecules further to obtain molecules with higher activity. In this study, it was tried to compare the inhibitory activities of the *P. harmala* molecules against the proteins of the SARS-CoV-2 virus. In this study, the proteins used are ACE2 protein ID: 6VW1 (33) of SARS-CoV-2 virus, main protease protein ID: 7BUY (34) of SARS-CoV-2 virus, and RNA-dependent RNA polymerase protein ID: 7BV2 (35) of SARS-CoV-2 virus. The inhibitory activities of the molecules contained in *P. harmala* against these proteins were compared. Many parameters were found in these docking calculations. Among these parameters, the parameter showing the inhibitory activity values of the molecules of *P. harmala* is the docking score. The molecule with the most negative numerical value of this

parameter has higher inhibitory activity than other molecules (36). The most important factor affecting the numerical values of the obtained docking score parameters is interaction. It has been observed that the numerical value of this parameter increases as the interaction increases. These interactions have many variations such as hydrogen bonds, polar and hydrophobic interactions, π - π , and halogen bonds (37–43). Three molecules with the highest inhibitory activity against ACE2 protein (6VW1), acacetin 7-O-rhamnoside of which docking score is -6.01 (AC7O), vasicine of which docking score is -5.73 (PubChem ID: 72610), harmol of which docking score is -5.55 (PubChem ID: 68094). The three molecules with the highest inhibitory activity against the main protease protein are vasicine of which docking score is -6.89 (PubChem ID: 72610), acacetin 7-O-rhamnoside of which docking score is -6.61 (AC7O), and harmol of which docking score is -5.96 (PubChem ID: 68094). The three molecules with the highest inhibitory activity against RNA-dependent RNA polymerase protein are harmol of which docking score is -7.28 (PubChem ID: 68094), vasicine of which docking score is -6.86 (PubChem ID: 72610), and norharman of which docking score is -6.66 (PubChem ID: 64961). The interactions of inhibitor molecules and proteins are given in Figures 3, 4, and 5.

Among the obtained docking score parameters, the most negative docking score parameter is -7.28 with the harmol molecule against RNA-dependent RNA polymerase protein. On the other hand, many more parameters of the molecules in *P. harmala* are calculated in the calculations. These parameters are the numerical values of the chemical and biological interactions of molecules. The glide ligand efficiency parameter is the numerical value of the effectiveness of molecules. Glide ecoul parameter shows the coulomb effect of inhibitor molecules (44). The glide emodel parameter is the numerical value of the model formed between the

Tab. 2. ADME properties of molecules.

	64961	68094	72610	AC7O	Reference range
mol_MW	168	198	188	414	130–725
dipole (D)	3.3	14.0	1.9	12.0	1.0–12.5
SASA	368	415	410	696	300–1000
FOSA	0	88	166	248	0–750
FISA	53	103	65	173	7–330
PISA	314	225	179	274	0–450
WPSA	0	0	0	0	0–175
volume (A ³)	587	672	665	1234	500–2000
donorHB	1	2	1	3	0–6
acceptHB	1.5	2.5	3.2	10.8	2.0–20.0
glob (Sphere =1)	0.9	0.9	0.9	0.8	0.75–0.95
QPpolrz (A ³)	20.3	22.9	21.5	42.0	13.0–70.0
QPlogPC16	6.7	7.2	6.4	13.6	4.0–18.0
QPlogPoct	8.8	15.5	9.8	25.8	8.0–35.0
QPlogPw	6.0	8.3	6.8	18.1	4.0–45.0
QPlogPo/w	2.3	1.8	1.9	1.5	–2.0–6.5
QPlogS	–2.4	–2.8	–2.4	–4.2	–6.5–0.5
CIQlogS	–2.7	–2.9	–2.3	–4.3	–6.5–0.5
QPlogHERG	–4.3	–4.3	–4.0	–6.1	*
QPPCaco (nm/sec)	3087	1048	2391	227	**
QPlogBB	0.1	–0.3	0.0	–1.6	–3.0–1.2
QPPMDCK (nm/sec)	1673	520	1270	100	**
QPlogKp	–1.4	–2.6	–2.0	–3.2	Kp in cm/hr
IP (ev)	8.4	7.3	8.5	9.1	7.9–10.5
EA (eV)	0.6	1.1	0.2	0.8	–0.9–1.7
#metab	2	3	2	4	1–8
QPlogKhsa	–0.1	–0.1	–0.2	–0.3	–1.5–1.5
Human Oral Absorption	3	3	3	3	–
Per. Human Oral Absorp.	100	91	100	78	***
PSA	27	57	38	120	7–200
RuleOfFive	0	0	0	0	Maximum is 4
RuleOfThree	0	0	0	0	Maximum is 3
Jm	26.5	0.7	5.7	0.0	–

*concern below –5, **a<25 is poor and a>500 is great, ***b<25 is poor and b>80 is high

inhibitor molecule and the protein (45). Glide posenum parameter is the numerical value of the exposure between the inhibitor molecule and the protein (46). All parameters calculated for interaction between inhibitor molecules and proteins are given in Table 1.

After molecular docking calculations of the molecules found in *P. harmala*, the inhibitory activities of 64961 (Norharman), 68094 (Harmol), 72610 (Vasicine), and AC7O (Acacetin 7-O-rhamnoside) molecules were found to be higher than other molecules. ADME/T calculations were made to predict the effects and responses of this molecule on human metabolism. These calculations have predicted the movement, action, and reaction of the molecules in organs and tissues in the human organism (46). Each parameter calculated gives different information about the molecules. The first parameter is mol_MW, which gives information about the molecular mass of the molecules. DonorHB parameter gives the numerical value of the hydrogen bonding ability of molecules. QPlogHERG parameter is the IC50 value related to the inhibition of HERG K⁺ channels. The QPPCaco parameter is used as a model of the blood-gut barrier. The unit of this parameter is nm/sec. The QPPMDCK parameter is the expression of the MDCK cell permeability in nm/sec for inactive transport. MDCK cells are a small model for the blood-brain barrier (47–50).

The last and most important two parameters are RuleOfFive (51, 52) and RuleOfThree (53). These two parameters are made up of many rules. The Rule of Five parameter, generally known as Lipinski's rule of five, consists of four parameters as mol_MW < 500, QPlogPo/w < 5, donorHB ≤ 5, acceptHB ≤ 10. The Rule of Three parameter, generally known as Jorgensen's rule of three, consists of three parameters such as QPlogS > –5.7, QP PCaco > 22 nm/s, #Primary Metabolites < 7 (Tab. 2).

As a result of the calculations, the activities of the inhibitor molecules of many SARS-CoV-2 viruses were compared. This comparison alone does not give clear information. Medicines approved by the US Food and Drug Administration (FDA) are used for bacteria, viruses, and many diseases for humans. For this reason, drugs used against the SARS-CoV-2 virus in the world, are ribavirin (PubChem number: 37542), arbidol (PubChem number: 131411), favipiravir (PubChem number: 492405), remdesivir (PubChem number: 121304016), clarithromycin (PubChem number: 84029), lopinavir (PubChem number: 92727), and azithromycin (PubChem number: 447043). Molecular docking calculations of these drugs were made against the ACE2 protein of the SARS-CoV-2 virus, the main protease protein, and the RNA-dependent RNA polymerase protein. As a result of the calculations, it is seen that PubChem ID: 68094 and 72610, AC7O inhibitor molecules have better inhibitory activity than FDA-approved drugs according to the docking score parameter. The numerical values obtained from the calculations made are given in Table 3. Among the FDA-approved drugs for the ACE2 protein (PDB ID: 6VW1) of the SARS-CoV-2 virus, the drug with the best numerical value of the docking score parameter of molecular docking calculations is lopinavir (PubChem number: 92727) with –5.01. Among the molecules in *P. harmala*, the inhibitor with the best docking score parameter is AC7O with –6.01. For another protein, the main protease protein, the best drug according to the docking score parameter of the FDA-approved drug is lopinavir (PubChem number: 92727) with –6.13. Among the molecules in *P. harmala*, the best inhibitor is PubChem ID: 72610 with –6.89. The final protein is ribavirin (PubChem number: 37542) with –6.94 for RNA-dependent RNA polymerase protein. Among the molecules in *P. harmala*, the best inhibitor is PubChem ID: 68094 with –7.28. As a result of the calculations made, it was observed that inhibitor molecules in *P. harmala* were higher than the FDA-approved drugs used.

The detailed calculations of the inhibitor molecules studied against the proteins of the SARS-CoV-2 virus were made by molecular docking and ADME/T calculations. In these calculations, the MM-PBSA calculations were made with the RNA-dependent RNA polymerase protein of the SARS-CoV-2 virus of the two molecules with the highest inhibitory activities. With these calculations, it was tried to suggest an ideal drug for the SARS-CoV-2 virus. The most effective FDA-approved drug of the RNA-dependent RNA polymerase protein of the SARS-CoV-2 virus is PubChem ID: 37542 (Ribavirin). In molecular docking calculations, the most effective inhibitors are PubChem ID: 68094 and 72610. Interaction energies up to 0-100 nanoseconds were examined in the calculations. Gibbs free energy change per 100 picoseconds between protein and inhibitors was calculated.

Tab. 3. Numerical values of the docking parameters of the molecule against enzymes.

Protein	Inhibitor	Docking score	Glide ligand efficiency	Glide evdw	Glide ecoul	Glide energy	Glide einternal	Glide emodel	Glide hBond
6VW1	92727	-5.10	-0.11	-43.29	-7.78	-51.07	15.65	-65.01	0.00
	492405	-4.67	-0.42	-14.83	-2.67	-17.50	0.03	-28.58	-0.16
	37542	-4.41	-0.26	-12.38	-12.04	-24.42	1.61	-31.72	-0.13
	121304016	-3.83	-0.09	-31.92	-5.79	-37.71	13.46	-46.82	-0.32
7BUY	131411	-3.44	-0.12	-27.21	-5.37	-32.58	2.02	-38.00	-0.32
	92727	-6.13	-0.13	-45.13	-7.17	-52.30	13.77	-68.86	-1.18
	37542	-5.30	-0.31	-24.42	-8.92	-33.34	6.27	-40.09	-2.24
	492405	-4.53	-0.41	-17.50	-8.09	-25.59	0.01	-33.10	-1.79
7BV2	37542	-6.94	-0.41	-15.81	-23.93	-39.74	3.44	-50.88	-4.38

Tab. 4. Gibbs binding free energy values in the interaction between inhibitor molecules and 7BV2 protein of the SARS-CoV-2 virus.

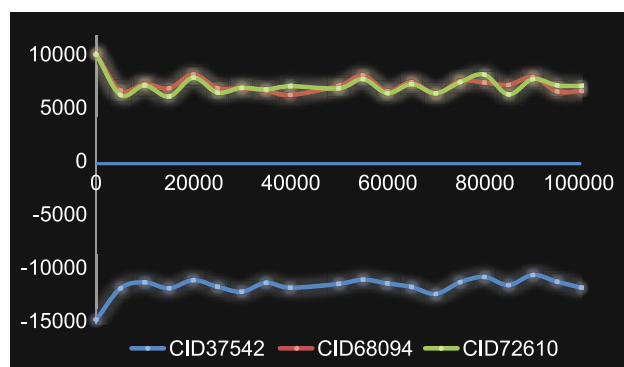
Time (ps)	CID37542	CID68094	CID72610
0	-14657.6	10306.1	10248.3
5000	-11687.9	6846.0	6430.7
10000	-11125.2	7453.7	7329.5
15000	-11679.8	7064.9	6299.7
20000	-10917.6	8360.6	8053.2
25000	-11531.9	7092.0	6663.2
30000	-12004.0	7060.7	7109.9
35000	-11159.6	6859.7	6951.6
40000	-11624.8	6443.4	7254.2
50000	-11268.4	7301.2	7060.1
55000	-10867.0	8265.4	7924.7
60000	-11218.1	6770.8	6600.3
65000	-11560.9	7625.7	7448.2
70000	-12205.8	6557.7	6601.6
75000	-11115.1	7740.0	7630.1
80000	-10618.1	7612.8	8339.3
85000	-11382.2	7382.4	6489.9
90000	-10435.5	8127.2	7921.4
95000	-11062.0	6776.7	7345.2
100000	-11624.0	6804.5	7282.4

Chem ID: 68094 and 72610 of the inhibitor molecules, which have the highest inhibitory activities in molecular docking calculations, are around +10200 and +10300, respectively. As the picoseconds pass, although the Gibbs free energy value of the inhibitor 37542 increases, the Gibbs free energy values of the inhibitor molecules 68094 and 72610 decrease. However, it appears that there is a large difference in energy between the average Gibbs free energy values between these two molecular groups.

Therefore, it is clear that the Gibbs free energy value of the FDA-approved drug (PubChem ID: 37542) is better than the studied inhibitor molecule value. Therefore, in molecular docking calculations for the SARS-CoV-2 virus, although the numerical value of the docking score parameter of the PubChem ID: 68094 inhibitor molecule is better than the PubChem ID: 37542 (Ribavirin) inhibitor, the PubChem ID: 37542 (Ribavirin) inhibitor's the Gibbs free energy appears to be better by a large margin in value.

Conclusion

The predominant molecules in the *P. harmala* leaves have been determined by experimental studies. Based on the experimental results, most alkaloids, flavonoids and triterpenoids found in *P. harmala* was compiled from the literature. The inhibitory activities of these inhibitor molecules against the SARS-CoV-2 virus against ACE2, main protease, and RNA-dependent RNA polymerase (RdRp) proteins were compared. It is the 68094 ID molecule with the best inhibitory activity against RNA-dependent RNA polymerase (RdRp) protein, which is -7.28 for the docking score parameter of this molecule. Although it is a better inhibitor than FDA-approved drugs according to molecular docking calculations, these calculations alone are not enough. MM-PBSA calculations were made with the RNA-dependent RNA polymerase (RdRp) protein of the 68094 ID molecule. Although the Gibbs free energy value of the molecule with ID 68094 averages 7422, the FDA-approved ribavirin is -11487. Although the inhibitory activity of 68094 is higher according to docking calculations, Gibbs free energy value is better than ribavirin. These results have been an important guide for future *in vivo* and *in vitro* procedures.

**Fig. 6. Exchange of Gibbs binding free energy values in the interaction between molecules and 7BV2 protein of the SARS-CoV-2 virus.**

Numerical values obtained from MM-PBSA calculations are given in Table 4 and Figure 6. In Table 4 and Figure 6, the Gibbs free energy value in the interaction of the SARS-CoV-2 virus with the RNA-dependent RNA polymerase protein of the drug PubChem ID: 37542 is -15000 in 0 nanoseconds. On the other hand, Pub-

References

1. **Pratama MRF, Nasibova TA, Pratiwi D et al.** *Peganum harmala* and its alkaloids as dopamine receptor antagonists: in silico study. *Biointerface Res Appl Chem* 2020; 11 (3): 10301–10316.
2. **Nasibova TA.** General characteristics of Syrian rue – *Peganum harmala*. *MAAM* 2019; 14 (3): 118–122.
3. **Toghyani M, Ghasemi A, Tabeidian SA.** The effect of different levels of seed and extract of Harmal (*Peganum harmala* L.) on immune responses of broiler chicks. *Int J Biol Biomol Agric Food Biotechnol Eng* 2015; 9 (1): 51–54.
4. **Quintana VM, Piccini LE, Panozzo ZJD et al.** Antiviral activity of natural and synthetic β -carbolines against dengue virus. *Antivir Res* 2016; 134: 26–33.
5. **Gonzalez MM, Cabrerizo FM, Baiker A et al.** β -carboline derivatives as novel antivirals for herpes simplex virus. *Int J Antimicrob Agents* 2018; 52 (4): 459–468.
6. **Edziri H, Mastouri M, Mahjoub MA et al.** Antibacterial, antiviral and antioxidant activities of aerial part extracts of *Peganum harmala* L. grown in Tunisia. *Toxicol Environ Chem* 2010; 92 (7): 1283–1292.
7. **Ma X, Liu D, Tang H et al.** Purification and characterization of a novel antifungal protein with antiproliferation and anti-HIV-1 reverse transcriptase activities from *Peganum harmala* seeds. *Acta Biochim Biophys Sin* 2012; 45 (2): 87–94.
8. **Singh B, Kaur P, Reid RJ et al.** COVID-19 and influenza co-infection: Report of three cases. *Cureus* 2020; 12 (8): e9852.
9. <https://www.cdc.gov/dengue/is-it-dengue-or-covid.html>
10. **Short WR.** Fatal herpes simplex virus type 2 pneumonia in a person with AIDS. *AIDS Read* 2009; 19 (2): 51–52.
11. **Fonseca B, Brune W, Stahl FR.** Cytomegalovirus (CMV) pneumonitis: Cell tropism, inflammation, and immunity. *Int J Mol Sci* 2019; 20 (16): 3865.
12. **Restrepo-Gualteros S, Jaramillo-Barberi L, Gonzalez-Santos M et al.** Characterization of cytomegalovirus lung infection in non-HIV infected children. *Viruses* 2014; 6 (5): 2038–2051.
13. **Richardson M, Elliman D, Maguire H et al.** Evidence base of incubation periods, periods of infectiousness and exclusion policies for the control of communicable diseases in schools and preschools. *Pediatr Infect Dis J* 2001; 20 (4): 380–391.
14. **Garbino J, Inoubli S, Mossdorf E et al.** Respiratory viruses in HIV-infected patients with suspected respiratory opportunistic infection. *AIDS* 2008; 22 (6): 701–705.
15. <https://www.cdc.gov/flu/about/professionals/genetic-characterization.htm>
16. **Diamond MS, Pierson, TC.** Molecular insight into dengue virus pathogenesis and its implications for disease control. *Cell* 2015; 162 (3): 488–492.
17. **Seitz R.** Human Immunodeficiency Virus (HIV). *Transfus Med Hemother* 2016; 43 (3): 203–222.
18. **Leveque N, Garcia M, Bouin A et al.** Functional consequences of RNA 5-Terminal deletions on coxsackievirus B3 RNA replication and ribonucleoprotein complex formation. *J Virol* 2017; 91 (16): e00423–17.
19. **Gao Q, Park MS, Palese P.** Expression of transgenes from newcastle disease virus with a segmented genome. *J Virol* 2008; 82 (6): 2692–2698.
20. **Nafisi S, Malekabady ZM, Khalilzadeh MA.** Interaction of β -carboline alkaloids with RNA. *DNA Cell Biol* 2010; 29 (12): 753–761.
21. **Goldsmith CS, Miller SE, Martines RB et al.** Electron microscopy of SARS-CoV-2: a challenging task. *Lancet* 2020; 395 (10238): e99.
22. **Moreno-Eutimio MA, López-Macías C, Pastelin-Palacios R.** Bioinformatic analysis and identification of single-stranded RNA sequences recognized by TLR7/8 in the SARS-CoV-2, SARS-CoV, and MERS-CoV genomes. *Microb Infect* 2020; 22 (4–5): 226–229.
23. **Shang J, Wan Y, Luo C et al.** Cell entry mechanisms of SARS-CoV-2. *Proceedings of the National Academy of Sciences* 2020; 117 (21): 11727–11734.
24. **Frisch MJ, Trucks GW, Schlegel HB et al.** 2009. Gaussian 09, revision D.01. Gaussian Inc, Wallingford CT
25. **Schrodinger L.** 2020. Small-Molecule Drug Discovery Suite 2020-4.
26. **Schrödinger Release 2020-4:** Protein Preparation Wizard; Epik, Schrödinger, LLC, New York, NY, 2016; Impact, Schrödinger, LLC, New York, NY, 2016; Prime, Schrödinger, LLC, New York, NY, 2020.
27. **Schrödinger Release 2020-4:** LigPrep, Schrödinger, LLC, New York, NY, 2020.
28. **Celebioglu HU, Erden Y, Hamurcu F et al.** Cytotoxic effects, carbonic anhydrase isoenzymes, α -glycosidase and acetylcholinesterase inhibitory properties, and molecular docking studies of heteroatom-containing sulfonyl hydrazone derivatives. *J Biomol Struct Dyn* 2020: 1–12.
29. **Schrödinger Release 2020-4:** QikProp, Schrödinger, LLC, New York, NY, 2020.
30. **Nelson MT, Humphrey, W, Gursoy A et al.** NAMD: A parallel, object-oriented molecular dynamics program. *Int J High Perform Comput Appl* 1996; 10 (4): 251–268.
31. **Humphrey W, Dalke A, Schulten K.** VMD: Visual molecular dynamics. *J Mol Graph* 1996; 14 (1): 33–38.
32. **Akkoc S, Tuzun B, Ilhan IO et al.** Investigation of structural, spectral, electronic, and biological properties of 1, 3-disubstituted benzimidazole derivatives. *J Mol Struct* 2020; 1219: 128582.
33. **Tuzun B, Saripinar E.** Molecular docking and 4D-QSAR model of methanone derivatives by electron conformational-genetic algorithm method. *J Iran Chem Soc* 2020; 17: 985–1000.
34. **Akin M, Günsel A, Bilgicli AT et al.** The Water-Soluble Peripheral Substituted Phthalocyanines as Corrosion Inhibitors for Copper in 0.1 N HCl: Gravimetric, Electrochemical, SEM-EDS, and Quantum Chemical Calculations. *Protect Met Phys Chem Surf* 2020; 56 (3): 609–618.
35. **Shang J, Ye G, Shi K. et al.** Structural basis of receptor recognition by SARS-CoV-2. *Nature* 2020; 581 (7807): 221–224.
36. **Jin Z, Zhao Y, Sun Y et al.** Structural basis for the inhibition of SARS-CoV-2 main protease by antineoplastic drug carmofur. *Nat Struct Mol Biol* 2020; 27 (6): 529–532.
37. **Yin W, Mao C, Luan X et al.** Structural basis for inhibition of the RNA-dependent RNA polymerase from SARS-CoV-2 by remdesivir. *Science* 2020; 368 (6498): 1499–1504.
38. **Tuzun B.** Examination of anti-oxidant properties and molecular docking parameters of some compounds in human body. *TC&TC* 2020; 4 (2): 76–87.
39. **Jayarajan R, Satheeshkumar R, Kottha T et al.** Water mediated synthesis of 6-amino-5-cyano-2-oxo-N-(pyridin-2-yl)-4-(p-tolyl)-2H-[1,2-bipyridine]-3-carboxamide and 6-amino-5-cyano-4-(4-fluorophenyl)-

- 2-oxo-N-(pyridin-2-yl)-2H-[1,2-bipyridine]-3-carboxamide – An experimental and computational studies with non-linear optical (NLO) and molecular docking analyses. *Spectrochim Acta A Mol Biomol Spectrosc* 2020; 229: 117861.
- 40. Sayin K, Ungordu A.** Investigations of structural, spectral and electronic properties of enrofloxacin and boron complexes via quantum chemical calculation and molecular docking. *Spectrochim Acta A Mol Biomol Spectrosc* 2019; 220: 117102.
- 41. Sayin K, Ungordu A.** Investigation of anticancer properties of caffeine complexes via computational chemistry methods. *Spectrochim Acta A Mol Biomol Spectrosc* 2018; 193: 147–155.
- 42. Sayin K.** Investigation of structural and biological properties of N-heterocyclic carbene silver (I) and palladium (II) complexes. *J Coord Chem* 2018; 71 (20): 3292–3303.
- 43. Ungordu A, Sayin K.** Quantum chemical calculations on sparfloxacin and boron complexes. *Chem Phys Lett* 2019; 733: 136677.
- 44. Aktas A, Nassif W, Sayin K.** Investigations of structural, spectral (IR, ¹H-, ⁹F-, ¹¹B-, ¹³C-, ¹⁵N-, ¹⁷O-NMR) and anticancer properties of 5FU@B₁₂N₁₂ complexes. *Chem Pap* 2021; 75: 1727–1737.
- 45. Ozdemir M, Koksoy B, Ceyhan D et al.** Design and in silico study of the novel coumarin derivatives against SARS-CoV-2 main enzymes. *J Biomol Struct Dyn* 2020: 1–16.
- 46. Aktas A, Tuzun B, Aslan R et al.** New anti-viral drugs for the treatment of COVID-19 instead of favipiravir. *J Biomol Struct Dyn* 2020: 1–11.
- 47. Aktas A, Tuzun B, Taskin AH et al.** How do arbidol and its analogs inhibit the SARS-CoV-2? *Bratisl Med J* 2020; 121 (10): 705–711.
- 48. Cetiner E, Sayin K, Tuzun B et al.** Could Boron-Containing Compounds (BCCs) be effective against SARS-CoV-2 as Anti-Viral Agent? *Bratisl Med J* 2021; 122 (4): 263–269.
- 49. Gezezen H, Gurdere MB, Dincer A et al.** Synthesis, molecular docking, and biological activities of new cyanopyridine derivatives containing phenylurea. *Arch Pharm* 2020; e2000334.
- 50. Huseynova A, Kaya R, Taslimi, P et al.** Design, synthesis, characterization, biological evaluation, and molecular docking studies of novel 1, 2-aminopropanthiols substituted derivatives as selective carbonic anhydrase, acetylcholinesterase and α -glycosidase enzymes inhibitors. *J Biomol Struct Dyn* 2020: 1–13.
- 51. Türkan F, Taslimi P, Abdalrazaq SM et al.** Determination of anticancer properties and inhibitory effects of some metabolic enzymes including acetylcholinesterase, butyrylcholinesterase, alpha-glycosidase of some compounds with molecular docking study. *J Biomol Struct Dyn* 2020: 1–10.
- 52. Gedikli MA, Tuzun B, Aktas A et al.** Are clarithromycin, azithromycin and their analogues effective in the treatment of COVID19? *Bratisl Med J* 2021; 122 (2): 101–110.
- 53. Taslimi P, Kocyigit UM, Tuzun B et al.** Biological effects and molecular docking studies of Catechin 5-O-gallate: antioxidant, anticholinergics, antiepileptic and antidiabetic potentials. *J Biomol Struct Dyn* 2020: 1–9.

Received February 22, 2021.

Accepted March 25, 2021.